

# Performance of X-ray grating interferometry at high energies

Matteo Abis, Thomas Thüring and Marco Stampanoni

*ETH Zürich and Paul Scherrer Institut*

## ABSTRACT

A theoretical description of the performance of a Talbot and Talbot-Lau type interferometers is developed, providing a framework for the optimization of the geometry for monochromatic and polychromatic beams. Analytical formulas for the smallest detectable refraction angle and the visibility of the setup are derived. The polychromatic visibility of the interference fringes is particularly relevant for the design of setups with conventional X-ray tubes, and it is described in terms of the spectrum of the source and the type of beam-splitter grating. We show the practical realization of such a design by imaging a metallic screw at 100 keV.

## 1. GRATING INTERFEROMETRY

Grating interferometry (figure 1) is an imaging technique yielding complementary signals from the interaction of X-rays with matter. Besides the absorption image, a phase shift<sup>1,2</sup> and a scattering<sup>3</sup> signal can be simultaneously retrieved from the interference pattern.

This approach does not rely on a highly coherent source, thus it can be applied to ordinary X-ray sources and not only to synchrotron facilities. The fundamental principle of this interferometric device is the Talbot self-imaging effect, where an image of a phase grating G1 is formed at certain distances downstream of the grating itself.

The phase sensitivity is given by the lateral displacement of the fringes in this interference pattern, corresponding to phase variations introduced by a sample in the direction  $x$ , perpendicular to the grating lines. The refraction angle  $\alpha$  is then:

$$\alpha = -\frac{1}{k} \frac{\partial \varphi}{\partial x}.$$

However, this displacement is so small for X-rays that the period of the fringes needs to be in the micrometer range. These fringes would not be visible at the resolution of typical medical imaging detectors. For this reason, an analyzer grating G2 with the same period as the interference pattern is installed in front of the detector. By scanning G2 along the  $x$  direction, the convolution between the interference pattern and the transmission profile of the grating itself is recorded on each pixel, yielding a *phase stepping curve*. Three parameters can be extracted by comparing the curve with the sample with a flat field image: the average value, related to the conventional absorption, the phase displacement, and the amplitude, which depends on the scattering.<sup>4</sup>

Finally, a grating interferometer can be set up on spatially incoherent and polychromatic sources, provided that a third grating G0 is introduced close to the X-ray tube.<sup>3,5,6</sup> This setup is known as a Talbot-Lau interferometer, where the source grating creates an array of individually coherent but mutually incoherent sources whose interference patterns are superimposed on the detector.

In order to achieve maximum performance, the design parameters of the interferometer, such as the pitch of the gratings and their position have to be tuned.

## 2. SENSITIVITY OPTIMIZATION

The fundamental parameter for the optimization of the geometry is the sensitivity, or smallest detectable refraction angle, given by:<sup>7</sup>

$$\sigma_\alpha = \frac{p_2}{\pi d} \frac{\sqrt{2}}{v} \sigma_{\text{det}},$$

where  $v$  is the visibility of the fringes, defined in this work as the ratio between the magnitudes of the first and zeroth Fourier coefficients of the phase stepping curve, and  $\sigma_{\text{det}}$  is the tipically poissonian noise introduced by

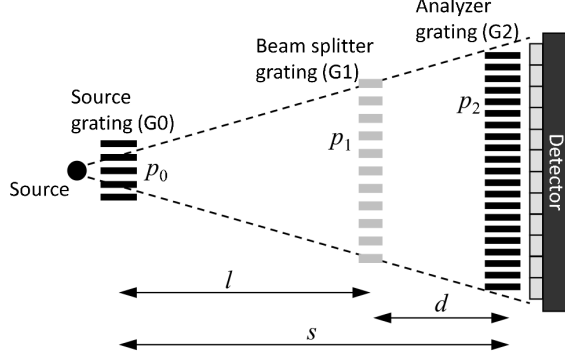


Figure 1: Parameters of a grating interferometer. The Talbot interferometer does not include a source grating G0.

the detector. The minimization of the smallest detectable refraction angle  $\alpha_{\min}^8$  for a Talbot interreferometer is achieved in two steps. The smallest source sizes  $w$  and analyzer grating periods should be chosen, according to the properties of the X-ray tube and the available grating technology. Then, an optimum period  $p_1$  of the beam-splitter grating can be calculated by minimizing  $\sigma_\alpha$ .

It can be shown that this is equivalent, for a  $\pi$ -shifting phase grating, to minimizing<sup>9</sup>

$$\sigma_\alpha \propto \frac{2p_2}{2p_2 - p_1} e^{\pi w \frac{2p_2 - p_1}{p_1 p_2}}.$$

For the Talbot-Lau design, on the other hand, the smallest  $\sigma_\alpha$  is achieved for the smallest sum of the pitches of G0 and G2. This is because the factor  $\sigma_\alpha \propto p_2/d$  can be rewritten, for a fixed total length  $s$ :

$$\frac{p_2}{d} = \frac{p_0 + p_2}{s}.$$

This ratio is limited by the grating fabrication. Since the process is the same for both the source and analyzer grating, this leads to the constraint  $p_0 = p_2$ , and a symmetric setup is the most sensitive.

### 3. OPTIMIZING THE DATA ANALYSIS

The analysis of the phase stepping curves is usually performed with Fast Fourier Transform algorithms applied to the phase steps recorded as G2 is displaced in front of the interference pattern. The first Fourier coefficient is then the absorption, the angle of the first coefficient is the phase displacement and the magnitude of the first coefficient is the amplitude of the curve. This algorithm is mathematically equivalent to an unweighted least squares fit.<sup>10</sup>

With a more computationally intensive procedure, each point can be weighted with the inverse of the poissonian variance given by the detector.

These two algorithms are compared through the simulation of sinusoidal phase stepping curves with nine steps each and purely poissonian noise  $\sigma_i = \sqrt{N_i}$ , where  $N_i$  is the number of counts for point  $i$ . To obtain statistically significant results, 100 000 curves for each mean value and visibility are generated.

The results of the statistical analysis of the simulation in figure 2a show the standard deviation of the reconstructed phase value as a function of visibility and for three values of the average intensity, which is proportional to the exposure time. For low visibilities, the poissonian weights are not very different for different phase stepping points. Thus the weighting does not improve the fit. The weighted estimators have minimum variance among all the linear estimators by the Gauss-Markov theorem<sup>11</sup> and a real difference appears for

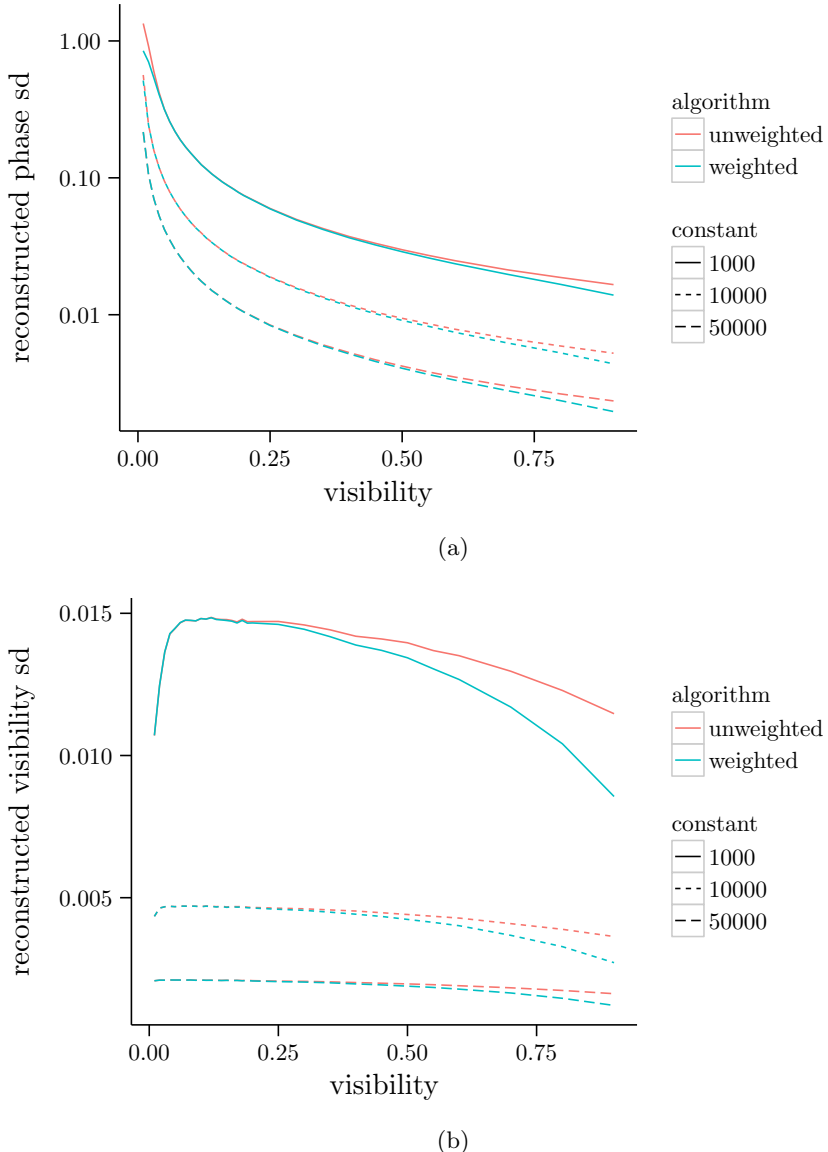


Figure 2: Comparison of the standard deviation of the phase (2a) and amplitude (2b) given by the Poisson variance in the detected number of hits for each phase stepping point.

visibilities above 50 %, which could only be reached in synchrotron experiments. This result could also be useful if other sources of noise can be determined, such as source instabilities.

On the other hand, the variance of the visibility (figure 2b) does not depend strongly on the visibility itself, but is inversely proportional to the exposure time. It is important to note here that, for very low counts, which occur for short exposure times or in areas with very high absorption, the visibility is biased (figure 3).<sup>12</sup> This occurs for both the weighted and unweighted fit algorithms.

These results show that the increased computational complexity of the weighted least squares fit can not be justified for experiments with lab sources, which can not reach a visibility above 50 % because of the low temporal coherence.

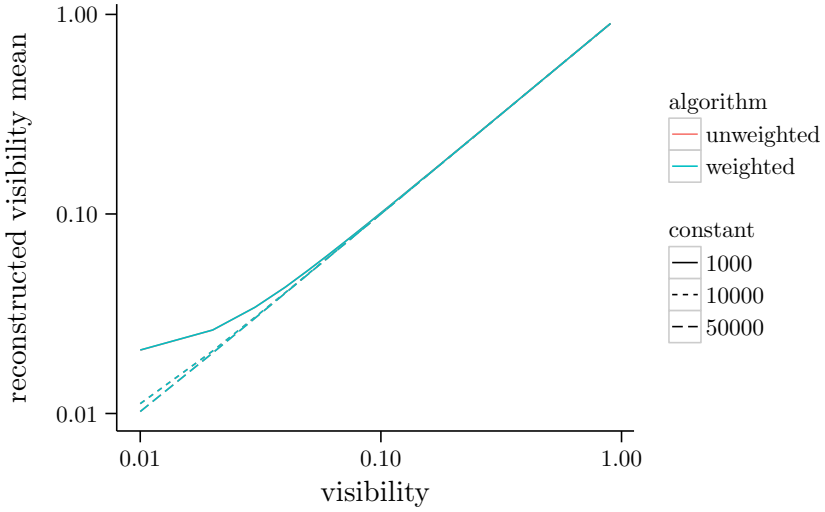


Figure 3: Bias of the reconstructed visibility for low detector counts.

#### 4. EXPERIMENTAL RESULTS

The results of these theoretical calculations have been used in the design of a Talbot-Lau interferometer for a high-energy X-ray tube (160 kVp) at the Paul Scherrer Institute (Switzerland).

The design energy of the interferometer is  $E_0 = 100$  keV, and the first Talbot distance was used to achieve the maximum spectral acceptance.<sup>13</sup> The setup is then symmetric with  $p_0 = p_1 = p_2 = 2.8\text{ }\mu\text{m}$  and an intergrating distance of 15.8 cm. At such high energies, only a 1D arrangement of the gratings is possible in order to overcome the limitations in the achievable aspect ratios of the gratings. Therefore, the beam is collimated onto a thin plane through a slit with a height of 100  $\mu\text{m}$ , and only one line of pixels is illuminated. The sample is then scanned across the slit to acquire a 2D radiograph.

The maximum theoretical visibility can be calculated according to<sup>9</sup>

$$v(\lambda) = \frac{2}{\pi} \left| \sin^2 \left( \frac{\lambda}{2\lambda_0} \right) \sin \left( \pi \frac{\lambda}{2\lambda_0} \right) \right|$$

$$v = \int v(\lambda) \rho(\lambda) d\lambda,$$

where  $\rho(\lambda)$  represents the spectrum of the source. The spectrum was simulated with SpekCalc,<sup>14</sup> resulting in a maximum theoretical visibility of 26 %. Figure 4 shows that the achieved visibility was much lower, about 5 %.

An SEM inspection revealed several problems with the manufacturing of the gratings, however, which can be responsible of this reduced performance. Several structures in the gratings are deformed and the duty cycle is not homogeneous. Other areas show an incomplete electroplating of the lamellae. Moreover, the grating mask is split into several regions, which can explain regular drops in visibility at the boundaries between these more homogeneous areas.

However, for a proof of principle the low visibility can be at least partially balanced by an increased exposure time, so that the noise is reduced.

Finally, the fundamental steps needed to optimize the design of a Talbot-Lau interferometer have been shown. The most relevant result is that the highest sensitivity is achieved for a symmetric setup. The maximum theoretical visibility is then calculated for a polychromatic spectrum, and an evaluation of the performance of the standard data analysis is compared to an optimal weighted fit. This shows that for a lab source with a wide spectrum, and therefore a maximum theoretical visibility around 30 %, the standard Fourier transform method is still reliable.

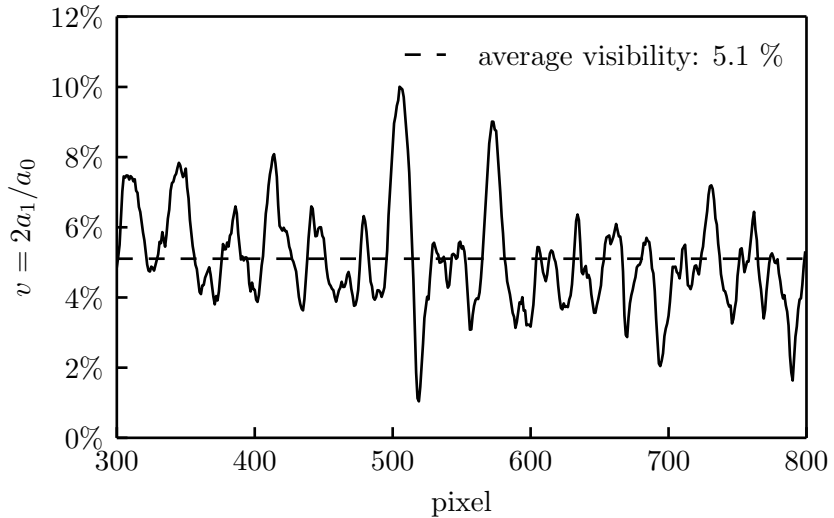


Figure 4: Visibility of the interferometer.

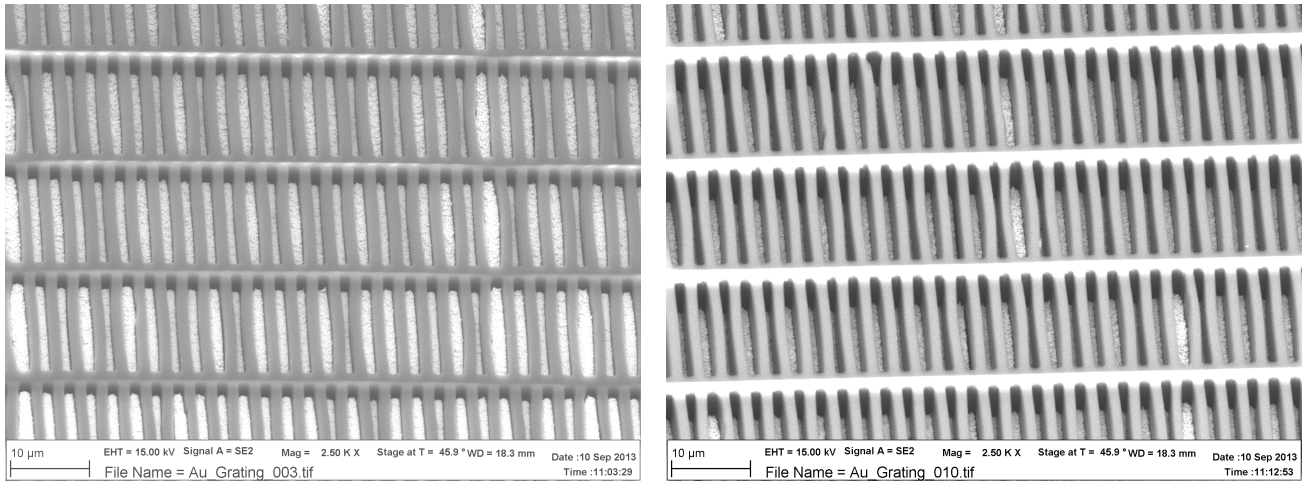


Figure 5: Scanning electron microscope images of the gratings. Figure 5a shows the irregularities in the duty cycle. Figure 5b shows some empty areas in the resist given by an incomplete electroplating.

The whole procedure was finally applied to the design of a Talbot-Lau interferometer at the Paul Scherrer Institute (Switzerland). The first images could be acquired despite several issues with the fabrication of the gratings.<sup>15</sup>

## Acknowledgements

We thank Gordan Mikuljan, Peter Modregger and Istvn Mohcsi from the Paul Scherrer Institute (PSI), Switzerland, for the work on the mechanical design, the scientific advice, and the SEM images respectively, Joachim Schulz and Marco Walter from Microworks GmbH, Germany, for the competent support on grating design issues, Christian Kottler and Vincent Revol from Centre Suisse d'Electronique et de Microtechnique (CSEM), Switzerland for the fruitful discussions on the design of the system. This work has been partially supported by the Competence Centre for Materials Science and Technology (CCMX) of the ETH Board, Project Nr. 61 and by the ERC Grant ERC-2012-StG 310005-PhaseX.

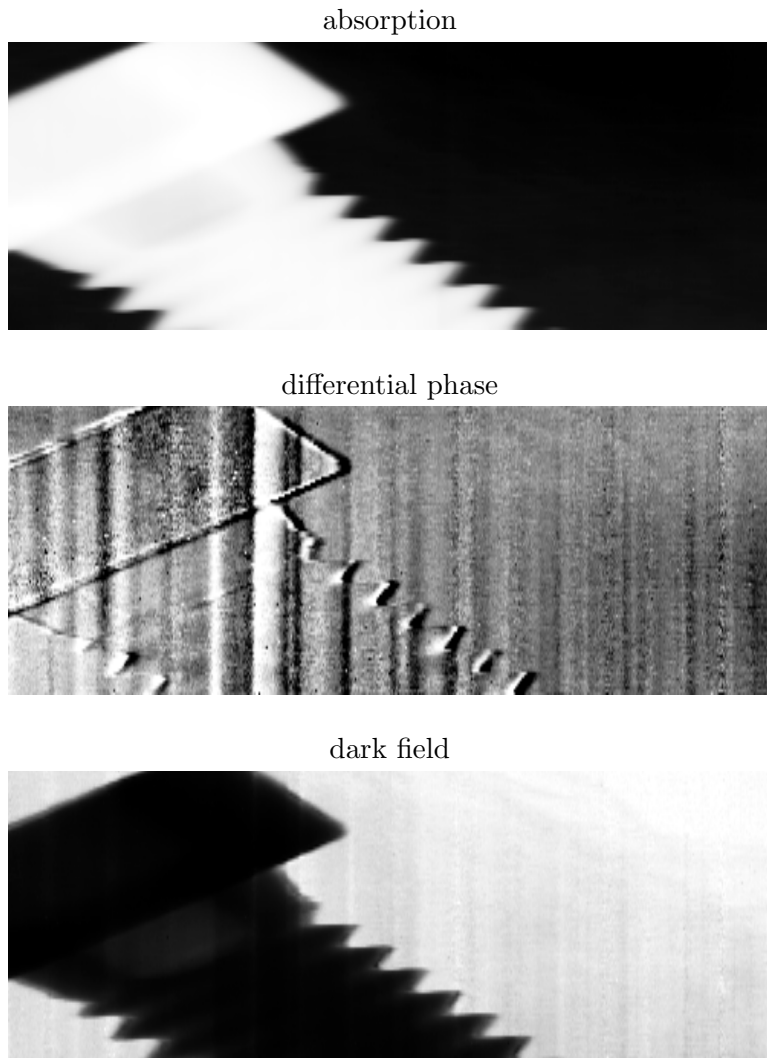


Figure 6: Radiograph of a zinc screw. The sample is scanned along 1 cm with 100 lines, 24 phase steps and 15 s exposure time per step.

## REFERENCES

- [1] David, C., Nöhammer, B., Solak, H., and Ziegler, E., “Differential x-ray phase contrast imaging using a shearing interferometer,” *81*(17), 3287–3289 (2002).
- [2] Momose, A., Kawamoto, S., Koyama, I., Hamaishi, Y., Takai, K., and Suzuki, Y., “Demonstration of X-Ray Talbot Interferometry,” *Japanese Journal of Applied Physics* **42**, L866–L868 (2003).
- [3] Pfeiffer, F., Weitkamp, T., Bunk, O., and David, C., “Phase retrieval and differential phase-contrast imaging with low-brilliance X-ray sources,” *Nature Physics* **2**, 258–261 (Mar. 2006).
- [4] Wang, Z., Kang, K. K.-J., Huang, Z.-F. Z., and Chen, Z.-Q. Z., “Quantitative grating-based x-ray dark-field computed tomography,” *Applied Physics Letters* **95**(9), 094105 (2009).
- [5] Chen, R. C., Longo, R., Rigon, L., Zanconati, F., De Pellegrin, a., Arfelli, F., Dreossi, D., Menk, R.-H., Vallazza, E., Xiao, T. Q., and Castelli, E., “Measurement of the linear attenuation coefficients of breast

- tissues by synchrotron radiation computed tomography.,” *Physics in Medicine and Biology* **55**, 4993–5005 (Sept. 2010).
- [6] Momose, A., Yashiro, W., Kuwabara, H., and Kawabata, K., “Grating-Based X-ray Phase Imaging Using Multiline X-ray Source,” *Japanese Journal of Applied Physics* **48**, 076512 (July 2009).
  - [7] Raupach, R. and Flohr, T. G., “Analytical evaluation of the signal and noise propagation in x-ray differential phase-contrast computed tomography.,” *Physics in Medicine and Biology* **56**, 2219–2244 (Mar. 2011).
  - [8] Thüring, T., Modregger, P., Hämmelerle, S., Weiss, S., Nüesch, J., and Stampanoni, M., “Sensitivity in X-ray grating interferometry on compact systems,” *AIP Conference Proceedings* **1466**(1), 293–298 (2012).
  - [9] Thüring, T. and Stampanoni, M., “Performance and optimization of x-ray grating interferometry,” *Philosophical Transactions of the Royal Society A: Mathematical, Physical and Engineering Sciences* **372**(2010) (2014).
  - [10] Scargle, J. D., “Studies in astronomical time series analysis. II - Statistical aspects of spectral analysis of unevenly spaced data,” *The Astrophysical Journal* **263**, 835–853 (Dec. 1982).
  - [11] Eadie, W. and James, F., [*Statistical Methods in Experimental Physics*], World Scientific (2006).
  - [12] Chabior, M., Donath, T., David, C., Schuster, M., Schroer, C., and Pfeiffer, F., “Signal-to-noise ratio in x-ray dark-field imaging using a grating interferometer,” *Journal of Applied Physics* **110**(5), 053105 (2011).
  - [13] Weitkamp, T., Diaz, A., David, C., Pfeiffer, F., Stampanoni, M., Cloetens, P., and Ziegler, E., “X-ray phase imaging with a grating interferometer,” *Optics Express* **13**(16), 6296–6304 (2005).
  - [14] Poludniowski, G., Landry, G., DeBlois, F., Evans, P., and Verhaegen, F., “SpekCalc: a program to calculate photon spectra from tungsten anode x-ray tubes.,” *Physics in Medicine and Biology* **54**, N433–N438 (Oct. 2009).
  - [15] Thüring, T., Abis, M., Wang, Z., David, C., and Stampanoni, M., “X-ray phase-contrast imaging at 100 kev on a conventional source,” *Scientific Reports* **4** (Jun 2014). Article.